

1

2

Helium optically pumped magnetometers can detect epileptic abnormalities

3

as well as SQUIDs as shown by intracerebral recordings

4

5 **Abbreviated title:**

6 Validation of Helium-OPM by simultaneous SEEG

7

8 **Authors:**

- 9 – Jean-Michel Badier: Aix Marseille Univ, INSERM, INS, Inst Neurosci Syst, Marseille, 13005, France
- 10 – Denis Schwartz: CERMEP-Imagerie du Vivant, MEG Departement, Lyon, 69003, France
- 11 – Christian-George Bénar: Aix Marseille Univ, INSERM, INS, Inst Neurosci Syst, Marseille, 13005,
12 France
- 13 – Khoubeib Kanzari: Aix Marseille Univ, INSERM, INS, Inst Neurosci Syst, Marseille, 13005, France
- 14 – Sébastien Daligault: CERMEP-Imagerie du Vivant, MEG Departement, Lyon, 69003, France
- 15 – Rudy Romain: CEA-LETI, MINATEC Campus, Univ. Grenoble Alpes, Grenoble, 38054, France;
16 MAG4Health, 9 Av Paul Verlaine 38100 Grenoble, 38000, France
- 17 – Sergey Mitryukovskiy: CEA-LETI, MINATEC Campus, Univ. Grenoble Alpes, Grenoble, 38054, France;
18 MAG4Health, 9 Av Paul Verlaine 38100 Grenoble, 38000, France
- 19 – William Fourcalt: CEA-LETI, MINATEC Campus, Univ. Grenoble Alpes, Grenoble, 38054, France
- 20 – Vincent Josselin: CEA-LETI, MINATEC Campus, Univ. Grenoble Alpes, Grenoble, 38054, France
- 21 – Matthieu Le Prado: CEA-LETI, MINATEC Campus, Univ. Grenoble Alpes, Grenoble, 38054, France;
22 MAG4Health, 9 Av Paul Verlaine 38100 Grenoble, 38000, France
- 23 – Julien Jung: CRNL, UMR_S 1028, INSERM, CNRS, Université Lyon 1, HCL, Lyon, 69002, France
- 24 – Augustin Palacios-Laloy: CEA-LETI, MINATEC Campus, Univ. Grenoble Alpes, Grenoble, 38054,
25 France; MAG4Health, 9 Av Paul Verlaine 38100 Grenoble, 38000, France
- 26 – Romain Carron: Aix Marseille Univ, INSERM, INS, Inst Neurosci Syst, Marseille, 13005, France ;
27 APHM, Timone hospital, Functional and Stereotactic Neurosurgery, Marseille, 1, 3005France
- 28 – Fabrice Bartolomei: Aix Marseille Univ, INSERM, INS, Inst Neurosci Syst, Marseille, 13005, France ;
29 APHM, Timone hospital, Epileptology and cerebral rythmology, Marseille, 13005, France
- 30 – Etienne Labyt: CEA-LETI, MINATEC Campus, Univ. Grenoble Alpes, Grenoble, 38054, France;
31 MAG4Health, 9 Av Paul Verlaine 38100 Grenoble, 38000, France

1 Francesca Bonini: Aix Marseille Univ, INSERM, INS, Inst Neurosci Syst, Marseille, 13005, France ;
2 APHM, Timone hospital, Epileptology and cerebral rythmology, Marseille, 13005, France

3 **Author Contributions:**

4 JMB, designed research, performed research, analyzed data, wrote the paper; FBo designed research,
5 analyzed data, wrote the paper, EL designed and performed research, wrote the paper; DS, FBa and CGB
6 wrote the paper; RC performed research; KK, RR, SM, APL, MLP, performed research; WF, VJ, SD, JJ
7 contributed unpublished analytic tools.

8

9 **Corresponding author:**

10 Francesca Bonini: Aix Marseille Univ, INSERM, INS, Inst Neurosci Syst, Marseille, 13005, France; APHM,
11 Timone hospital, Epileptology and cerebral rythmology, Marseille, 13005, France
12 francesca.bonini@univ-amu.fr

13

14

15 **Abstract**

16

17

18 SQUID-based magnetoencephalography has been shown to improve the diagnosis and surgical treatment
19 decision for presurgical evaluation of drug-resistant epilepsy. Still, its use remains limited due to several
20 constraints such as cost, fixed helmet size and obligation of immobility. A new generation of sensors, the
21 optically pumped magnetometers (OPMs), could overcome these limitations. In this study, we validate the
22 ability of innovative Helium-based OPM (⁴He-OPM) sensors to record epileptic brain activity thanks to
23 simultaneous recordings with intracerebral EEG (stereotactic EEG, SEEG). We recorded simultaneous
24 SQUIDs-SEEG and 4He-OPM-SEEG signals in one patient during two sessions. We show that epileptic
25 activities on intracerebral EEG can be recorded by OPMs with a better signal-to noise ratio than classical
26 SQUIDs. The OPM sensors open new venues for the widespread application of magnetoencephalography in
27 the management of epilepsy and other neurological diseases and fundamental neuroscience.

28

29 **Significance Statement:**

30 We performed a simultaneous recording of Helium-based Optically Pumped Magnetometers (OPM) and
31 intracerebral EEG and validate for the first time OPM results with signals recorded directly within the brain.
32 We demonstrate that epileptic abnormalities seen on intracerebral electrodes are detected by OPMs with a
33 better signal-to noise ratio than classical magnetoencephalography. This represents a significant step

- 1 towards the validation of OPM-based recordings for epilepsy diagnosis and for clinical and neuroscience
- 2 research.

1 Introduction

2

3 Magnetoencephalography (MEG) is a non-invasive, millisecond-resolution source imaging technique for
4 recording and localizing brain signals. The analysis of magnetic brain activity allows for a
5 deeper understanding of the neural substrates of brain pathologies. In the management of drug-resistant
6 epilepsy, MEG contributes to the success of surgical treatment through non-invasive localization of
7 interictal epileptic discharges (IEDs) and can also guide the implantation of depth electrodes when invasive
8 recordings are required [Fischer et al., 2005; Murakami et al., 2016].

9 Still, the spread of MEG is strongly limited by the constraints imposed by the use of superconducting
10 quantum interference devices (SQUIDs)[Cohen, 1972; Hämäläinen et al., 1993], requiring cooling at very
11 low temperature (4.2 K). Thus, the sensors are isolated and enclosed in a fixed array inside a rigid dewar, at
12 least 3 cm from the brain. The critical consequences are a substantial reduction in the magnetic signal
13 amplitude, inhomogeneous coverage, and the need for total immobility during signal acquisition.

14 The emergence of a new generation of MEG sensors, the optically-pumped magnetometers (OPM)[Budker
15 and Romalis, 2007], could overcome these limitations. OPM are quantum sensors that exploit the
16 interaction between an atomic gas and laser light to obtain very precise measurements of tiny magnetic
17 fields.. OPM do not require extreme cooling, and can be placed near the scalp in a wearable system thus
18 allowing subject's movement [Boto et al., 2017; Iivanainen et al., 2017; Johnson et al., 2013] [Boto et al.,
19 2018; Boto et al., 2022; Seymour et al., 2021]. The development and improvement of this new technology
20 has taken a quantum leap in recent years, with evolution in miniaturization and sensitivity (for complete
21 reviews see [Brookes et al., 2022; Labyt et al., 2022; Tierney et al., 2019]). The first commercially available
22 OPMs, based on Alkali atoms[Budker and Romalis, 2007], have a sensitivity of 20fT/rtHz in tri-axis mode
23 compared to 5 fT/rtHz for SQUID sensors. However, their placement close to the scalp allows a 3-8 fold
24 increase in signal power [Budker and Romalis, 2007; Iivanainen et al., 2017; Johnson et al., 2013], with a
25 significant neuromagnetic signal enhancement compared to SQUIDs, namely for superficial sources[Boto et
26 al., 2016; Boto et al., 2017; Iivanainen et al., 2017].

27 More recently, new OPMs based on Helium atoms (⁴He-OPMs) have been developed[Beato et al., 2018],
28 having a large dynamic range (up to 250 nT) and a large frequency bandwidth (up to 2kHz) with negligible
29 heat dissipation (10 mW per sensor). Their properties allow recording in a standard magnetic shielding
30 room, facilitating data acquisition.

31 A few studies have shown that alkali OPMs can record IEDs comparable to those observed with SQUID-
32 MEG [Feys et al., 2022] or previously obtained EEG [Vivekananda et al., 2020]. However, to compare OPM
33 to SQUID-MEG, it is necessary to ensure that both modalities are recording equivalent IEDs. By using

1 stereotactic intracerebral-EEG (SEEG) as a groundtruth, simultaneously recorded with OPMs and
2 SQUIDs[Badier et al., 2017], we aimed to demonstrate that ⁴He-OPMs can perform as well as SQUID-MEG
3 but at an expected lower cost and with greater convenience. These unique simultaneous recordings
4 allowed selecting similar IEDs to compare SQUID-MEG and ⁴He-OPM and thus evaluate the Signal to Noise
5 Ratio (SNR) of both techniques.

6

7

8 **Methods**

9 The simultaneous recordings were performed inside a 2-layer μ -metal magnetic shielded-room (MSR) on a
10 patient with drug-resistant focal epilepsy undergoing SEEG. Fourteen intracerebral electrodes with a total
11 of 119 recording contacts were implanted mainly in the left temporal structures (Fig. 1d). These electrodes,
12 and particularly those exploring the anterior medial and lateral temporal regions, disclosed abundant
13 interictal epileptic abnormalities. A first SQUID-MEG/SEEG recording session (Fig. 1a) of 20 minutes at rest
14 was followed by a comparable ⁴He-OPM/SEEG session. The four ⁴He-OPM sensors (2 x 2 x 5 cm) fixed on a
15 rigid helmet (Fig. 1b) were placed over the left central and temporal regions, in contact with the bandage
16 covering the scalp (Fig. 1c, red dots). The four SQUID sensors closest to the four ⁴He-OPMs sensors were
17 selected for analysis and for comparison with the magnetic activity recorded by the OPM sensors (Fig. 1c,
18 green dots). These four SQUIDs were between 2.72 cm and 3.23 cm away from the OPM sensors.

19

20 **Patient:** The patient (age range 31-35 years old) suffered from intractable temporal epilepsy. A stereo-EEG
21 (SEEG) was performed to define the EZ to be removed. Most electrodes (12/14) were aimed at an extensive
22 exploration of the left temporal structures, as well as the anterior insula and the orbito-frontal cortex; two
23 electrodes were implanted in the right anterior temporal region. At the end of the SEEG, the epileptogenic
24 zone network could be defined as involving the left mesial temporal structures including the amygdala,
25 hippocampus, rhinal cortex, left parahippocampal cortex and collateral sulcus (the latter being posterior to
26 the cavernoma) and the left temporal pole. The simultaneous recording session was carried out at the end
27 of the long-term video-SEEG recording, at J11 from electrodes implantation once all clinical data were
28 acquired. The ethical approval was obtained at the XXXX under ID RCB 2020-A01830-39 and the patient
29 gave informed consent.

30 **SEEG recordings:** SEEG exploration was performed using intracerebral multiple contacts electrodes placed
31 intracranially with robotic assistance (ROSA, Zimmer Biomet) and intraoperative Mobius-Airo CT-scan
32 (Stryker, US) verification. Small insertion screws (2023-VG-C-10 or -15, Alcis Besancon) were used to
33 minimize the bulk of the electrodes around the skull and to allow for simultaneous recordings. The
34 electrodes had a diameter of 0.8 mm, contained 10 to 15 contacts. Each contact consists of 2 mm long

1 platinum-iridium and separated from each other by 1.5 mm of insulated material (XXXXX). To accurately
2 define the anatomical position of each SEEG contact along the electrode trajectory, a CT-scan/MRI data
3 fusion was performed using the in-house software XXXX. This Matlab-based tool is able to co-register the
4 MRI to the CT-scan, and to automatically segment and localize depth electrodes contacts by image
5 processing. The signals were formatted in a bipolar configuration keeping only non-contiguous bipolar
6 channels. Recording was made with a BrainProducts BrainAmp DC amplifier. SEEG data have been sampled
7 at 2500Hz.

8 **SQUID-MEG recordings:** The first recording was done with a SQUID MEG system simultaneously with the
9 SEEG (see above) in supine position. MEG Signals were acquired on a 4D Neuroimaging™ 3600 whole head
10 system at a sampling rate of 2034.51 Hz with a total of 248 magnetometers. Additionally, 3 magnetometers
11 and 9 gradiometers were used for noise compensation. The electrocardiographic and the
12 electrooculographic activity were recorded on bipolar EEG channels. SQUID-MEG/SEEG recording was done
13 in supine position.

14 **⁴He-OPM recordings:** The second recording were done with a prototype of five ⁴He-OPM sensors
15 simultaneously with SEEG, also in supine position. The ⁴He-OPMs are sensors that measure the brain
16 magnetic field along the three axes with a continuous self-compensation of the magnetic field on all axes.
17 The magnetic field measurement relies on a measure of the variation of the light absorption caused by the
18 deviation of the electronic spin of ⁴He atoms from the state originally set by a laser pumping. Technical
19 information and physical principles used in our sensors can be found in a previous publication [XXXXX] and
20 are summarized below. The OPM used in this study is based on parametric resonance of helium-4
21 metastable atoms at near zero magnetic field [Beato et al., 2018; Dupont-Roc, 1971]. The cell containing the
22 ⁴He gas is a cylinder of 1 cm diameter and 1 cm height. This cell, placed at the bottom of the sensor, is
23 surrounded by small 3-axis Helmholtz coils which are used to apply both the RF fields and the
24 compensation fields (see below). A High-Frequency (HF) discharge (excited between 10 and 20 MHz and
25 consuming around 10 mW power) excites the ⁴He atoms from their ground state to the metastable triplet
26 state which has three Zeeman sublevels. A selective optical pumping (with a linearly polarized beam tuned
27 on the D0 line at 1083 nm) is performed to prepare a macroscopic magnetic moment on the gas, which
28 evolves in the magnetic field created by the brain. In our OPMs, to derive a vector measurement of the
29 three components of the magnetic field, two RF fields are applied to the gas: $B_{\Omega} \cos \Omega t$ along one tangential
30 X axis and $B_{\Omega} \cos \Omega t$ along the radial Y axes. Both are orthogonal to polarization of the pump laser beam.
31 Thanks to this scheme first introduced by Dupont-Roc [Dupont-Roc, 1971], three resonance signals are
32 detected on the transmitted pump light at Ω , Ω , and $\Omega \pm \Omega$. To first order, the amplitude of each resonance is
33 respectively proportional to one of the three components of the magnetic field to be measured
34 (respectively Bx, By, and Bz).

1 Each sensor is operated in a closed-loop mode on the three axes. This consists in continuously cancelling
2 the three components of the magnetic field by applying an opposite field with the 3-axis Helmholtz coils.
3 The value of each magnetic field component is deduced from the current injected in the compensation coil.
4 In this way the sensor becomes self-calibrated, i.e. its output can only be affected by variations of the
5 transfer function between current and magnetic field set by the coil geometry, and not by other operating
6 parameters (light intensity, HF power...). This closed-loop mode suppresses the cross-axis effects[Cohen-
7 Tannoudji et al., 1970a; Cohen-Tannoudji et al., 1970b; Dupont-Roc, 1970; Dupont-Roc, 1971] by which the
8 measurement of one axis becomes dependent of the field along another axis. This phenomenon has been
9 recently referred as the Cross-Axis Projection Error (CAPE)[Borna et al., 2022], yielding both phase errors
10 and a tilt of the sensing axis. Previous studies with alkali OPM operated in an open-loop mode have
11 characterized an axis tilt of $3.3^\circ/\text{nT}$ at low frequencies[Borna et al., 2022] and offsets as small as 1.5 nT
12 resulted in gain errors of $\sim 5\%$ [Boto et al., 2018]. Thereby, ^4He OPM is the first sensor, to our knowledge, to
13 provide a measurement of the magnetic field components in a closed-loop mode along the three axes,
14 guaranteeing the reliability of the measurement and avoiding any CAPE. Another important advantage of
15 closed-loop operation is the possibility of broadening the dynamic range well above the atomic linewidth. A
16 dynamic range of $\pm 250\text{nT}$ is currently achieved for our ^4He OPMs. The sensitivity of our magnetometer
17 operating in the closed-loop tri-axial mode is better than $50 \text{ fT/Hz}^{1/2}$ on two of the three axes (the radial and
18 one tangential) with a bandwidth going from DC to 2 kHz.

19 However, if the closed-loop mode avoids CAPE, it has some unwanted consequences due to the cross-talks
20 that unavoidably exist between the sensors within the OPM array. This problem can be solved by
21 appropriate post-processing as far as the cross-talks are appropriately characterized (for a detailed
22 description, see XXXX). The measured cross-talk matrix for an array of four ^4He OPM sensors with only 2-
23 mm spacing, which corresponds to an extremely unfavourable situation as compared to a real OPM MEG
24 set-up, revealed low cross-talk ($<10\%$) and showed a good agreement with the estimated matrix from the
25 Biot-Savart calculations. Knowing this cross-talk matrix, minor cross-talk related errors are corrected in the
26 measurement by adequate post-processing. OPM data have been sampled at 11161 Hz and downsampled
27 to 4 kHz.

28

29 ***OPM, SQUID and SEEG spatial Co-registration:***

30 The spatial co-registration was performed for both sessions using a 3D Polhemus digitizer, based on three
31 fiducial markers (nasion, left and right pre-auricular points). The quality of the co-registration was checked
32 using the digitization of the facial mask. Following the standard procedure for 4D Neuroimaging, the
33 position of nasion and both tragi were digitized to allow the construction of the patient frame. The
34 positions of 5 coils located on the subject's head were also digitized. Activations of these 5 coils before and

1 after recording allowed to determine the location of the MEG sensors within the patient frame. For the ^4He
2 OPM-MEG/SEEG session, the same three fiducial markers were digitized in the same reference frame. In
3 this case, the sensors were linked to the subject head by the ^4He OPM headset. This headset was
4 positioned on the subject head prior to the insertion of the ^4He OPM sensors and the corresponding slots
5 were digitized giving the location of each ^4He OPM sensor within the same patient reference frame. Finally,
6 both types of sensors were localized in the same reference frame, i.e. the subject head. It was then possible
7 to select the SQUID sensors closest to each ^4He OPM based on Euclidean distance.

8

9 ***Data processing:***

10 Noise correction: A noise compensation was performed for SQUIDs thanks to recordings from reference
11 sensors (magnetometers and gradiometers). Noise compensation is obtained by subtracting the
12 contribution of the noise measured by the references for each sensor. As there are not enough sensors to
13 perform it, there is no such compensation for the OPM. In that case noise cancellation is only performed by
14 filtering (band-pass filter 2Hz-70Hz and a notch filter at 50Hz). Downsampling and temporal registration:
15 since the data were acquired with different devices, post-processing was necessary to temporally register
16 the simultaneous recordings with the same sampling rate and the same number of samples. To do so,
17 randomly distributed triggers were sent to both kind of MEG sensors (SQUID or OPM) and SEEG. Data were
18 then processed by an in-house Matlab routine to match the sequence of triggers and to resample the data
19 (from SEEG to MEG time frame). The resampling procedure did not result in differences in delays larger
20 than 1 sample. The end results for each session (SQUID-SEEG and OPM-SEEG) were two files that contained
21 the same number of samples with synchronized SEEG and MEG data. Filtering: all data were band-pass
22 filtered at 2-70Hz; a notch filter at 50Hz was added. SNR computation: to investigate the amplitude of
23 events, the SNR was computed as the following ratio: the max amplitude of the event divided by the
24 standard deviation of a baseline (2s of signal before the event for the single event presented in Fig. 2 and
25 500ms for the averages in Fig. 3 and Fig. 4).

26 Automatic extraction of events of interest: We had to compare data recorded in the two separate sessions.
27 To do so, we used a procedure to identify identical events across recordings. As a first step, an expert
28 neurologist (FB) manually selected four kinds of events of interest from the SEEG recording of the SQUID
29 session. The selection was done using a montage of one bipolar SEEG derivation per explored brain areas.
30 These “reference” events were chosen to be representative of IEDs involving lateral temporal structures
31 (Spike I) and IEDs involving both medial and lateral temporal structures (Spike II). We used the Matlab
32 routine « findsignal » (Matlab 2020b) to find similar intracerebral events for both the SQUID session and
33 the OPM session. Three to ten events were kept for averaging. From this set of events, we chose a
34 representative occurrence of Spike II to illustrate a single event (See Fig. 1).

1 Results

2 As a main result, the analysis of the simultaneous recordings globally shows that the activities recorded by
3 the intracerebral electrodes placed in the left temporal pole are detected on the scalp surface by both
4 systems, conventional SQUID-MEG and OPM-MEG (Fig. 2, 3, 4). Notably ⁴He-OPM-MEG recordings showed
5 an SNR better than that of SQUID-MEG.

6 Single interictal events (epileptic spikes), are visible on both OPM and SQUID recordings. Fig. 2 presents
7 single epileptic spikes with the corresponding SEEG traces. Using band-pass filtering (2 Hz to 70 Hz) and a
8 notch filter (50 Hz) with no further processing, the ⁴He-OPM-MEG can clearly record, with a high signal-to-
9 noise ratio (SNR), the IEDs identified with the SEEG electrodes. A single epileptic spike arising from the left
10 temporal pole and the adjacent anterior third temporal gyrus (Fig. 2c shows the intracerebral traces), is
11 distinctly identified on the scalp by the ⁴He-OPM-MEG (SNR=7, peak-to-peak amplitude=5pT) (Fig. 2d). In
12 comparison, the four closest SQUID-MEG sensors, using advanced denoising based on reference sensors,
13 detect an equivalent intracerebral spike (visible on simultaneous SEEG in Fig. 2a) but with a lower SNR of 5
14 (Fig. 2b). This can be explained by the reduced distance from the neuronal sources of ⁴He-OPM-MEG,
15 yielding increased signal power compared to SQUID-MEG [Labyt et al., 2019]. Furthermore, it is interesting
16 to note that different time courses and polarities are clearly identifiable, depending on the location of the
17 channel and the orientation of the magnetic field (Fig. 2d). The ⁴He-OPM sensors are natively sensitive to
18 two orthogonal orientations of the magnetic field, so that two different signals corresponding to the
19 tangential and radial components (red lines and blue lines, respectively, in Fig. 2d) are output for each
20 sensor.

21 These results observed on single spikes are even more evident when comparing the average of ⁴He-OPM-
22 MEG and SQUID-MEG signals (Fig. 3). In order to compare a sufficient number of equivalent epileptic events
23 recorded by OPMs and SQUID, we manually identified, using a selective SEEG electrodes montage, four
24 different types of epileptic spikes recorded in the two separate simultaneous sessions (for details see
25 Methods session and Supplementary Fig. 1 and 2). These IEDs have been subsequently automatically
26 extracted from the entire time series and averaged by type. Two types of IEDs are illustrated, an average
27 spike arising from the left temporal pole only (Fig. 3a and c, red line) and an average spike arising from the
28 temporal pole, the third anterior temporal gyrus (minimally), and the anterior hippocampus (Fig. 4a and c,
29 red, orange, and blue line, respectively). In both cases, the simultaneous SQUID-MEG averaged data reveal
30 a small deflection (Fig. 3b and 4b, respectively -6pT and 3.7pT max value) in correspondence with the
31 averaged intracerebral spikes (Fig. 3a and 4a). In contrast, the ⁴He-OPM-MEG averaged data disclose clear
32 averaged spikes (Fig. 3d and 4d) occurring along with the two averaged intracerebral spikes (Fig. 3c and 4c).
33 Both ⁴He-OPM-MEG spikes have a higher amplitude (spike I=-9.5 pT; spike II=-10pT) and a higher SNR (spike
34 I: SNRr=6.4; spike II: SNRr=16.7) than those detected in the SQUID-MEG data. Regarding averaged spike-II,

1 it is interesting to note that the time course of the OPM signal appears to be correlated with the decay of
2 the temporo-polar spike, as recorded by electrode TP' 3-4, whereas the hippocampal activity recorded by
3 electrode B' 2-3 is not detected by MEG sensors, neither by SQUIDs nor by OPMs. On the other hand,
4 variable time-courses, polarities, and amplitudes between radial and tangential measurement axes can be
5 observed on the OPM signals, particularly on spike II (Fig. 4d). The radial components of the two anterior
6 sensors show a negative deflection while for the corresponding tangential components, the deflection is
7 positive and slightly delayed. This suggests that ⁴He-OPM-MEG provides more information than SQUID-
8 MEG about the spatio-temporal organisation of IEDs across the cerebral cortex thanks to their tangential
9 component.

10

11 **Discussion**

12

13

14 In this study we report the results of two sets of simultaneous intracerebral recordings of IEDs, one with
15 ⁴He-OPM-MEG and the other one with SQUID-MEG. Using SEEG as reference and ground-truth, we
16 correlated the IEDs recorded by intracerebral electrodes with both ⁴He-OPM and SQUID sensors. We
17 obtained the first direct validation of the ability of ⁴He-OPM sensors to record epileptic activities and we
18 demonstrate that new ⁴He-OPM system has better performance to record IEDs than SQUID-MEG system, as
19 evidenced by its higher SNR. Notably, these recordings have been achieved in a regular clinical
20 environment, without advanced noise correction. Thanks to their native 3D measurement of the magnetic
21 field, OPM signals disclose variations in time-courses, polarities, and amplitudes between the radial and
22 tangential components of the recorded activity.

23 Simultaneous acquisition of MEG and intracerebral EEG is a technical feat [Dalal et al., 2009; Dubarry et al.,
24 2014; Santiuste et al., 2008] but can now be performed without major difficulties [Badier et al., 2017]. It
25 has several key advantages in comparison with separate acquisition. It allows capturing the same activity at
26 the surface and in depth, avoiding potential differences in brain state and medication. This is particularly
27 important for IEDs that are spontaneous events which can widely vary in extent from one event to the
28 other [Badier and Chauvel, 1995]. Simultaneity allows correlating signals across events [Dubarry et al., 2014]
29 and in the current study, allowed finding similar events to be compared in SQUID and OPM sessions based
30 on the SEEG topography. With this reliable comparison, we can establish that ⁴He-OPMs are at least as
31 capable of recording epileptic activity as SQUIDs.

32 Currently, alkali-based OPM are mainly used for MEG recordings in healthy volunteers (for a review, see
33 [Brookes et al., 2022]) and few studies in epileptic patients have been performed [Tierney et al., 2021;
34 Vivekananda et al., 2020] [Feys et al., 2022], with one seizure recording recently reported [Feys et al.,

1 2023]. Present results strengthen the perspective that OPMs are an accurate and valid alternative to
2 SQUIDs.

3 Nonetheless, although very promising, clinical adoption of OPMs remains challenging due to some
4 limitations of the current technology. Alkali OPMs have a limited bandwidth (1-100 Hz) and a small dynamic
5 range (5 nT), requiring higher attenuation than a conventional shielded room for SQUID-MEG, demanding a
6 complementary system of magnetic shielding coils to compensate for the remaining magnetic field and to
7 reduce the cross-talk. Another challenge posed by the heat dissipation by sensors must be solved, possibly
8 with a helmet design including insulation and/or cooling. Despite these constraints and thanks to
9 technological advances to overcome them, alkali-based OPMs have given numerous proofs of their good
10 sensitivity to biomagnetic measurements [Brookes et al., 2022; Labyt et al., 2019; Tierney et al., 2019]. As
11 evidence of the rapid evolution of the technology, 90-channel OPM systems offering triaxial magnetic field
12 detection have been shown to improve cortical coverage successfully [Boto et al., 2022; Rea et al., 2022].
13 The additional information offered by a vectorial measurement of the magnetic field, also reported in the
14 present study, will be of interest to better characterize the spatio-temporal dynamics of the epileptic
15 activity and to interpret clinical data [Iivanainen et al., 2017; Zahran et al., 2022]. In our study, the delay of
16 the tangential component (see averaged spike-II) is potentially informative on the propagation of the
17 interictal activity, as shown by comparing radial SQUID-MEG and EEG [Merlet et al., 1997].

18 Helium-based OPMs could overcome some of the limitations of alkali OPM, as they can be placed nearest
19 the scalp without any discomfort for the patient, since they do not require thermal insulation. ^4He -OPM
20 are currently the only sensors to be self-compensated on their three measurement axes in a closed loop
21 operating mode, ensuring a highly reliable measurement of the brain magnetic field, without cross-axis
22 projection error [Fourcault et al., 2021], and bringing better stability of the sensors scale factor along time.
23 This also allows for an increased dynamic range (up to 250 nT), larger than the one corresponding to the
24 helium resonance linewidth, which eliminates the constraint of a strict field nulling system: in this study,
25 ^4He -OPMs have been used in a standard two-layer MSR in the hospital environment, known to be
26 particularly magnetically “noisy”. On the other hand, in their current release, ^4He -OPMs have a worse
27 sensitivity (40 fT/rtHz) [Fourcault et al., 2021] compared to alkali ones (20 fT/rtHz in tri axis mode) [Boto et
28 al., 2022]. However, in a recent study in a large group of healthy subjects, the ^4He -OPMs showed very
29 similar results to the classical SQUID-MEG system thanks to their shorter distance to the brain [Gutteling et
30 al., 2023]. In our study, we observed that ^4He -OPM can record IEDs with a better SNR compared to SQUIDs.
31 This result altogether with the recent data from 18 volunteers shows that ^4He -OPMs are able to deliver
32 high quality brain recordings [Gutteling et al., 2023].

33 Some limitation of this work comes from the limited number of OPM sensors. Nevertheless, the full
34 coverage of the SQUID system allowed selecting of the co-localized SQUID sensors and ensuring a

1 reasonable comparison. We found that the amplitude of the OPM signals was higher than that of SQUID
2 signals, as expected from both simulations and real data[Boto et al., 2016; Boto et al., 2017; Iivanainen et
3 al., 2017]. Still, the MEG IEDs, measured with 4He-OPMs and SQUIDs, arose from neocortical structures.
4 We could not show activity from deep structures - such as the hippocampus - on either type of sensor.
5 Sensitivity to deep sources remains a challenge. It will be necessary to use a larger number of sensors to
6 verify if source separation techniques such as independent component analysis will allow to extract activity
7 from deep sources as previously demonstrated[Pizzo et al., 2019].

8 With all its advantages, OPM technology could extend the use of MEG to many clinical and research
9 applications. Currently, only very few clinical centres have a MEG facility. By offering more affordable cost,
10 higher signal sensitivity and bandwidth, and portability without additional equipment, the OPM technology
11 paves the way for the democratization of this unique non-invasive method of high-resolution brain
12 exploration, potentially powerfully impacting both clinical practice and neuroscience.

13

14

15

16

17

18

19

1 **References**

- 2 Badier JM, Chauvel P (1995): Spatio-temporal characteristics of paroxysmal interictal events in human
3 temporal lobe epilepsy. *J Physiol* 89:255–264.
4 <https://www.sciencedirect.com/science/article/pii/0928425796836424>.
- 5 Badier JM, Dubarry AS, Gavaret M, Chen S, Trébuchon AS, Marquis P, Régis J, Bartolomei F, Bénar CG,
6 Carron R (2017): Technical solutions for simultaneous MEG and SEEG recordings: towards routine
7 clinical use. *Physiol Meas* 38:N118. <https://dx.doi.org/10.1088/1361-6579/aa7655>.
- 8 Beato F, Belorizky E, Labyt E, Le Prado M, Palacios-Laloy A (2018): Theory of a He 4 parametric-resonance
9 magnetometer based on atomic alignment. *Phys Rev A* 98.
- 10 Borna A, Iivanainen J, Carter TR, McKay J, Taulu S, Stephen J, Schwindt PDD (2022): Cross-Axis projection
11 error in optically pumped magnetometers and its implication for magnetoencephalography systems.
12 *Neuroimage* 247:118818. <https://doi.org/10.1016/j.neuroimage.2021.118818>.
- 13 Boto E, Bowtell R, Krüger P, Fromhold TM, Morris PG, Meyer SS, Barnes GR, Brookes MJ (2016): On the
14 potential of a new generation of magnetometers for MEG: A beamformer simulation study. *PLoS One*
15 11:1–24.
- 16 Boto E, Holmes N, Leggett J, Roberts G, Shah V, Meyer SS, Muñoz LD, Mullinger KJ, Tierney TM, Bestmann S,
17 Barnes GR, Bowtell R, Brookes MJ (2018): Moving magnetoencephalography towards real-world
18 applications with a wearable system. *Nature* 555:657–661. <http://dx.doi.org/10.1038/nature26147>.
- 19 Boto E, Meyer SS, Shah V, Alem O, Knappe S, Kruger P, Fromhold TM, Lim M, Glover PM, Morris PG, Bowtell
20 R, Barnes GR, Brookes MJ (2017): A new generation of magnetoencephalography: Room temperature
21 measurements using optically-pumped magnetometers. *Neuroimage* 149:404–414.
- 22 Boto E, Shah V, Hill RM, Rhodes N, Osborne J, Doyle C, Holmes N, Rea M, Leggett J, Bowtell R, Brookes MJ
23 (2022): Triaxial detection of the neuromagnetic field using optically-pumped magnetometry:
24 feasibility and application in children. *Neuroimage* 252.
- 25 Brookes MJ, Leggett J, Rea M, Hill RM, Holmes N, Boto E, Bowtell R (2022): Magnetoencephalography with
26 optically pumped magnetometers (OPM-MEG): the next generation of functional neuroimaging.
27 *Trends Neurosci* 45:621–634. <https://doi.org/10.1016/j.tins.2022.05.008>.
- 28 Budker D, Romalis M (2007): Optical magnetometry. *Nat Phys* 3:227–234.
- 29 Cohen-Tannoudji C, Dupont-Roc J, Haroche S, Laloë F (1970a): Diverses résonances de croisement de
30 niveaux sur des atomes pompés optiquement en champ nul I. Théorie. *Rev Phys Appl* 5:95–101.
- 31 Cohen-Tannoudji C, Dupont-Roc J, Haroche S, Laloë F (1970b): Diverses résonances de croisement de
32 niveaux sur des atomes pompés optiquement en champ nul II. Applications à la mesure de champs
33 faibles. *Rev Phys Appl* 5:102–108.
- 34 Cohen D (1972): Magnetoencephalography: detection of the brain's electrical activity with a
35 superconducting magnetometer. *Science* 175:664–666.
- 36 Dalal SS, Baillet S, Adam C, Ducorps A, Schwartz D, Jerbi K, Bertrand O, Garnero L, Martinerie J, Lachaux JP
37 (2009): Simultaneous MEG and intracranial EEG recordings during attentive reading. *Neuroimage*
38 45:1289–1304.
- 39 Dubarry A-S, Badier J-M, Trébuchon-Da Fonseca A, Gavaret M, Carron R, Bartolomei F, Liégeois-Chauvel C,
40 Régis J, Chauvel P, Alario F-X, Bénar C-G (2014): Simultaneous recording of MEG, EEG and
41 intracerebral EEG during visual stimulation: from feasibility to single-trial analysis. *Neuroimage*
42 99:548–558.

- 1 Dupont-Roc J (1970): Détermination par des méthodes optiques des trois composantes d'un champ
2 magnétique très faible. *Rev Phys* 5:853–864.
- 3 Dupont-Roc J (1971): Etude théorique de diverses résonances observables en champ nul sur des atomes
4 'habillés' par des photons de radiofréquences. *J Phys* 32:135–144.
- 5 Feys O, Corvilain P, Aeby A, Sculier C, Christiaens F, Holmes N, Brookes M, Goldman S, Wens V, De Tiège X
6 (2022): On-Scalp Optically Pumped Magnetometers versus Cryogenic Magnetoencephalography for
7 Diagnostic Evaluation of Epilepsy in School-aged Children. *Radiology* 304:429–434.
- 8 Feys O, Corvilain P, Van Hecke A, Sculier C, Rikir E, Legros B, Gaspard N, Leurquin-Sterk G, Holmes N,
9 Brookes M, Goldman S, Wens V, De Tiège X (2023): Recording of Ictal Epileptic Activity Using on-Scalp
10 Magnetoencephalography. *Ann Neurol* 93:419–421.
- 11 Fischer MJM, Scheler G, Stefan H (2005): Utilization of magnetoencephalography results to obtain
12 favourable outcomes in epilepsy surgery. *Brain* 128:153–157.
- 13 Fourcault W, Romain R, Le Gal G, Bertrand F, Josselin V, Le Prado M, Labyt E, Palacios-Laloy A (2021):
14 Helium-4 magnetometers for room-temperature biomedical imaging: toward collective operation and
15 photon-noise limited sensitivity. *Opt Express* 29:14467.
- 16 Gutteling TP, Bonnefond M, Clausner T, Daligault S, Romain R, Mitryukovskiy S, Fourcault W, Josselin V, Le
17 Prado M, Palacios-Laloy A, Labyt E, Jung J, Schwartz D (2023): A New Generation of OPM for High
18 Dynamic and Large Bandwidth MEG: The (4)He OPMs-First Applications in Healthy Volunteers. *Sensors*
19 (Basel) 23.
- 20 Hämäläinen M, Hari R, Ilmoniemi RJ, Knuutila J, Lounasmaa O V. (1993): Magnetoencephalography theory,
21 instrumentation, and applications to noninvasive studies of the working human brain. *Rev Mod Phys*
22 65:413–497.
- 23 Iivanainen J, Stenroos M, Parkkonen L (2017): Measuring MEG closer to the brain: Performance of on-scalp
24 sensor arrays. *Neuroimage* 147:542–553. <http://dx.doi.org/10.1016/j.neuroimage.2016.12.048>.
- 25 Johnson CN, Schwindt PDD, Weisend M (2013): Multi-sensor magnetoencephalography with atomic
26 magnetometers. *Phys Med Biol* 58:6065–6077.
- 27 Labyt E, Sander T, Wakai R (2022): Flexible High Performance Magnetic Field Sensors: On-Scalp
28 Magnetoencephalography and Other Applications. Springer International Publishing.
29 <https://books.google.fr/books?id=8H-FEAAAQBAJ>.
- 30 Labyt E, Corsi M-C, Fourcault W, Palacios Laloy A, Bertrand F, Lenouvel F, Cauffet G, Le Prado M, Berger F,
31 Morales S (2019): Magnetoencephalography With Optically Pumped (4)He Magnetometers at
32 Ambient Temperature. *IEEE Trans Med Imaging* 38:90–98.
- 33 Merlet I, Paetau R, García-Larrea L, Uutela K, Granström ML, Mauguière F (1997): Apparent asynchrony
34 between interictal electric and magnetic spikes. *Neuroreport* 8:1071–1076.
- 35 Murakami H, Wang ZI, Marashly A, Krishnan B, Prayson RA, Kakisaka Y, Mosher JC, Bulacio J, Gonzalez-
36 Martinez JA, Bingaman WE, Najm IM, Burgess RC, Alexopoulos A V. (2016): Correlating
37 magnetoencephalography to stereo-electroencephalography in patients undergoing epilepsy surgery.
38 *Brain* 139:2935–2947.
- 39 Pizzo F, Roehri N, Medina Villalon S, Trébuchon A, Chen S, Lagarde S, Carron R, Gavaret M, Giusiano B,
40 McGonigal A, Bartolomei F, Badier JM, Bénar CG (2019): Deep brain activities can be detected with
41 magnetoencephalography. *Nat Commun* 10:1–13. <http://dx.doi.org/10.1038/s41467-019-08665-5>.
- 42 Rea M, Boto E, Holmes N, Hill R, Osborne J, Rhodes N, Leggett J, Rier L, Bowtell R, Shah V, Brookes MJ

- 1 (2022): A 90-channel triaxial magnetoencephalography system using optically pumped
2 magnetometers. *Ann N Y Acad Sci* 1517:107–124.
- 3 Santiuste M, Nowak R, Russi A, Tarancon T, Oliver B, Ayats E, Scheler G, Graetz G (2008): Simultaneous
4 magnetoencephalography and intracranial EEG registration: technical and clinical aspects. *J Clin*
5 *Neurophysiol Off Publ Am Electroencephalogr Soc* 25:331–339.
- 6 Seymour RA, Alexander N, Mellor S, O'Neill GC, Tierney TM, Barnes GR, Maguire EA (2021): Using OPMs to
7 measure neural activity in standing, mobile participants. *Neuroimage* 244:118604.
8 <https://doi.org/10.1016/j.neuroimage.2021.118604>.
- 9 Tierney TM, Holmes N, Mellor S, López JD, Roberts G, Hill RM, Boto E, Leggett J, Shah V, Brookes MJ,
10 Bowtell R, Barnes GR (2019): Optically pumped magnetometers: From quantum origins to multi-
11 channel magnetoencephalography. *Neuroimage* 199:598–608.
- 12 Tierney TM, Levy A, Barry DN, Meyer SS, Shigihara Y, Everatt M, Mellor S, Lopez JD, Bestmann S, Holmes N,
13 Roberts G, Hill RM, Boto E, Leggett J, Shah V, Brookes MJ, Bowtell R, Maguire EA, Barnes GR (2021):
14 Mouth magnetoencephalography: A unique perspective on the human hippocampus. *Neuroimage*
15 225:117443.
- 16 Vivekananda U, Mellor S, Tierney TM, Holmes N, Boto E, Leggett J, Roberts G, Hill RM, Litvak V, Brookes MJ,
17 Bowtell R, Barnes GR, Walker MC (2020): Optically pumped magnetoencephalography in epilepsy. *Ann*
18 *Clin Transl Neurol* 7:397–401.
- 19 Zahran S, Mahmoudzadeh M, Wallois F, Betrouni N, Derambure P, Le Prado M, Palacios-Laloy A, Labyt E
20 (2022): Performance Analysis of Optically Pumped ^4He Magnetometers vs. Conventional SQUIDs:
21 From Adult to Infant Head Models. *Sensors* 22:1–18.
- 22
- 23

1 **Figures' legends**

2

3 **Fig. 1. SQUID-MEG, ⁴He-OPM-MEG and SEEG recording setup.** *a) and b) items have been removed from this MedXriv*
4 *submission as required for preventing any possible person identification. readers Please contact the corresponding*
5 *author to request access to these materials.* a) Simultaneous SQUID-MEG/SEEG: the classic cryogenic MEG system,
6 measuring 120 cm x 100 cm and weighting about 300 Kg, with 265 SQUID sensors in a fixed array requiring subject
7 immobility during data acquisition. b) Simultaneous ⁴He-OPM-MEG/SEEG: recording configuration composed of 4
8 sensors integrated in a wearable helmet placed on the scalp and in contact with the bandage covering the SEEG
9 electrodes inserts (the cables and connectors coming out of the helmet are visible). In the top left insert is a picture of
10 the ⁴He-OPM sensor. c) 3D reconstruction of the patient's head from MRI, with ⁴He-OPM (in red), SQUID sensors (in
11 blue) and SEEG electrodes entry points (in orange). The 4 SQUID sensors, closest to the OPMs, are coloured in green.
12 Note the distance between the SQUIDs and the scalp (at least 3 cm), while the ⁴He-OPM are in contact with it. d) SEEG
13 implantation: 14 intracerebral electrodes, 2 in the right hemisphere (not shown) and 12 in the left hemisphere
14 exploring the whole left temporal structures: A': amygdala, TP': temporal pole; TB': rhinal cortex; B' anterior
15 hippocampus; C': posterior hippocampus; GPH': para-hippocampal gyrus; T': anterior insula/lateral T1; H':
16 thalamus/Heschl gyrus gyrus; Ia': anterior insula/F2; FCA': lingual gyrus; GC': posterior cingulate/T1; OR' orbito-frontal
17 cortex/middle frontal sulcus

18

19 **Fig. 2: Individual spikes results.** The left side of the figure presents the signal collected during the SQUID-MEG/SEEG
20 simultaneous session: **a.** Bipolar SEEG data. The name of the SEEG electrodes and the recording contact label are
21 shown. The labels range from 1 (deeper location) to 11 (most surface location). The spike clearly involves both deep
22 and more superficial structures (amygdala, anterior and posterior hippocampus, third anterior temporal gyrus and
23 temporal pole). **b.** Simultaneous SQUID-MEG data collected on the four sensors closest to the ⁴HeOPM channels: an
24 interictal epileptic spike appears around 82.5s, with peak-to-peak amplitude of 1.1pT. The right side of the figure
25 presents the signal collected during the ⁴He-OPM-MEG/SEEG simultaneous session. **c.** Bipolar SEEG data. Note the
26 similarity between two intracerebral spikes disclosing the same anatomical location and time course. **d.** Simultaneous
27 ⁴He-OPM-MEG data collected on four sensors: t=tangential magnetic field (red lines) and r=radial magnetic field (blue
28 lines). A spike appears at 342.5s with a peak-to-peak amplitude of 2,5 pT. The vertical scale is identical to that of the
29 SQUID data on the left.

30

31 **Fig. 3: Averaged Type I spikes (n=10).** The left side of the figure presents the averaged signal collected during the
32 SQUID-MEG/SEEG simultaneous session, the right side presents the averaged signal collected during the ⁴He-OPM-
33 MEG/SEEG simultaneous session. The name of the SEEG electrodes and recording contacts are shown. Contacts range
34 from 1 (deeper location) to 9 (most surface location). **a,** Bipolar averaged SEEG data for the SQUID session. The
35 averaged spike involves only the bipolar TP'3-TP'4 recording (Temporal pole). **b,** Simultaneous SQUID-MEG averaged
36 data on the four sensors closest to the ⁴HeOPM sensors: a small interictal spike appears around 25ms with a peak-to-
37 peak amplitude of 8 pT. **c,** Bipolar averaged SEEG data for the OPM session. Note the similarity between the

1 intracerebral spikes of the two sessions, disclosing the same anatomical location and time course. **d**, ^4He -OPM-MEG
2 averaged data collected on four sensors (T_{pos} , C_{ant} , C_{post} , T_{ant}). The subscript indicates the orientation: T tangential
3 magnetic field (dashed lines), R radial magnetic field (solid lines). A spike appears at 35ms with a maximum peak-to-
4 peak amplitude of 15 pT. The vertical scale is identical to that of the SQUID data on the left.

5 **Fig 4: Averaged Type II spikes (n=3)**. Similar figure arrangement to that of Fig. 3. **a**, Bipolar averaged SEEG data for the
6 SQUID session. The spikes involve a larger network encompassing TP', TB' and B' electrodes (medial and lateral
7 temporal pole, anterior hippocampus, third anterior temporal gyrus). **b**, Simultaneous SQUID-MEG averaged data on
8 the four sensors closest to the ^4He -OPM sensors: a very faint spike appears around 75ms with a peak-to-peak
9 amplitude of 4 pT. **c**, Bipolar averaged SEEG data for the OPM session. Note the similarity between the intracerebral
10 spikes of the two sessions, disclosing the same anatomical location and time course. **d**, ^4He -OPM-MEG averaged data
11 collected on four sensors (T_{pos} , C_{ant} , C_{post} , T_{ant}). The subscript indicates the orientation: T tangential magnetic field
12 (dashed lines), R radial magnetic field (solid lines). A spike appears at 75s with a peak-to-peak amplitude of 9.3 pT
13 maximum. The vertical scale is identical to that of the SQUID data on the left.

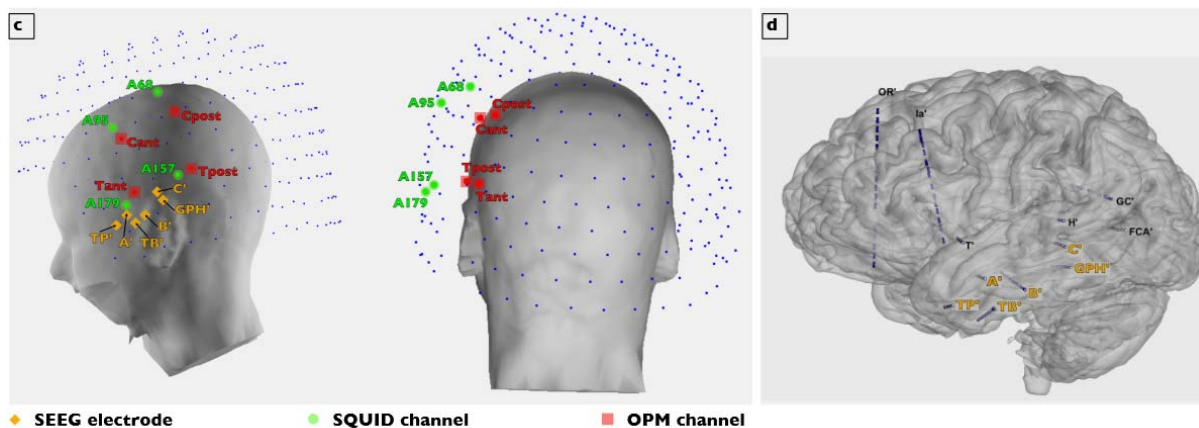
14

15

Figures

16

17 **Fig. 1**



18

19

20

21

22

23

24

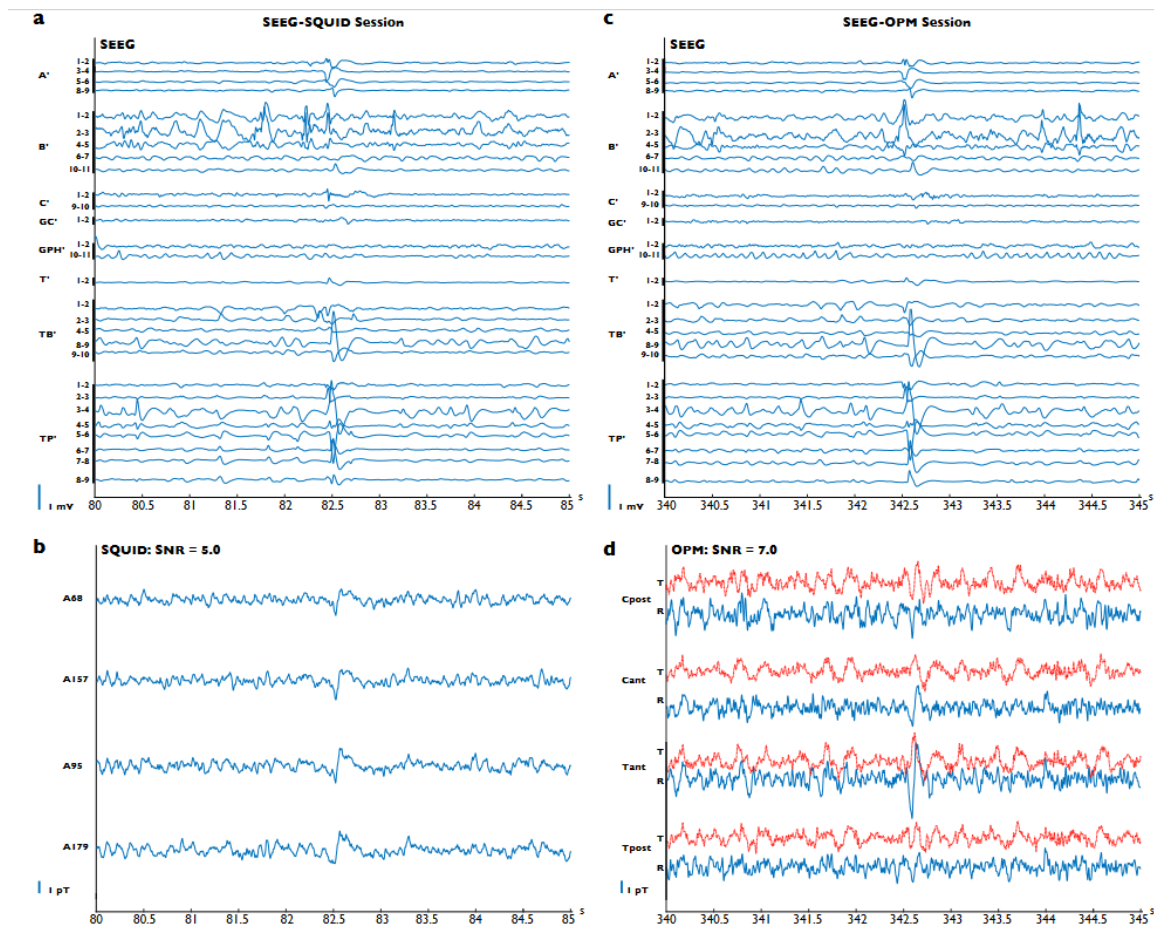
25

26

1

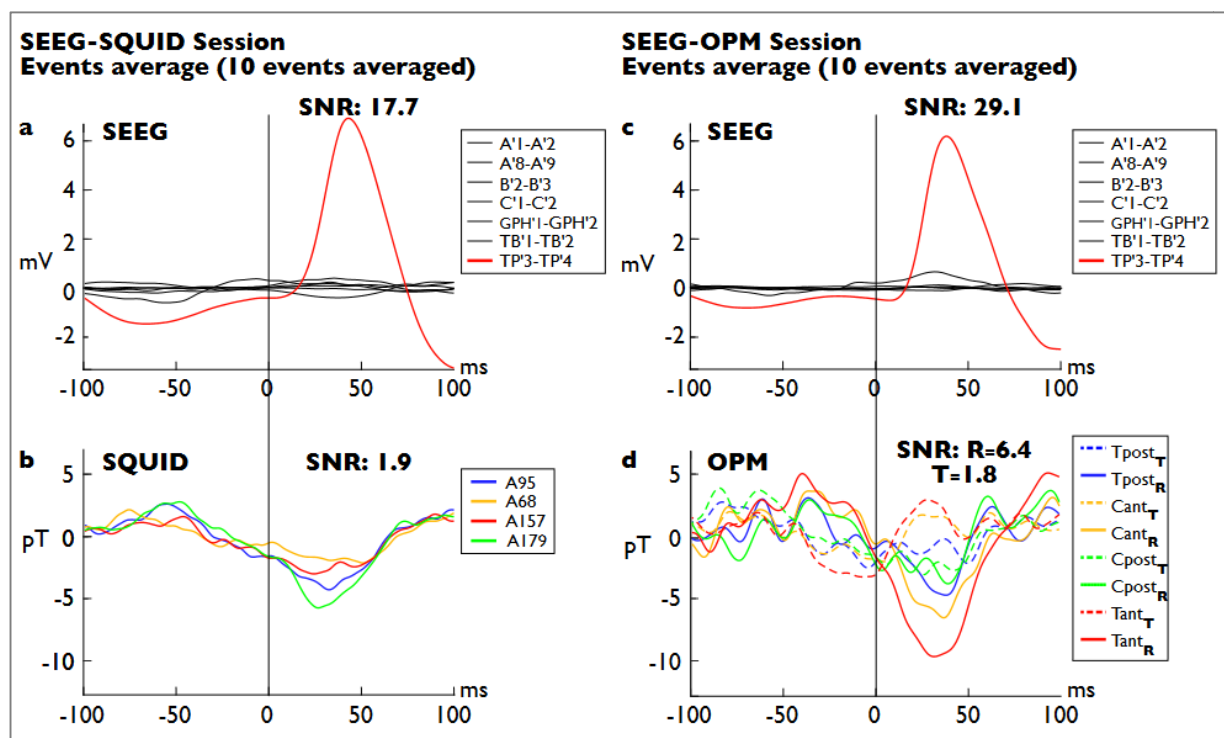
2

3 Fig. 2



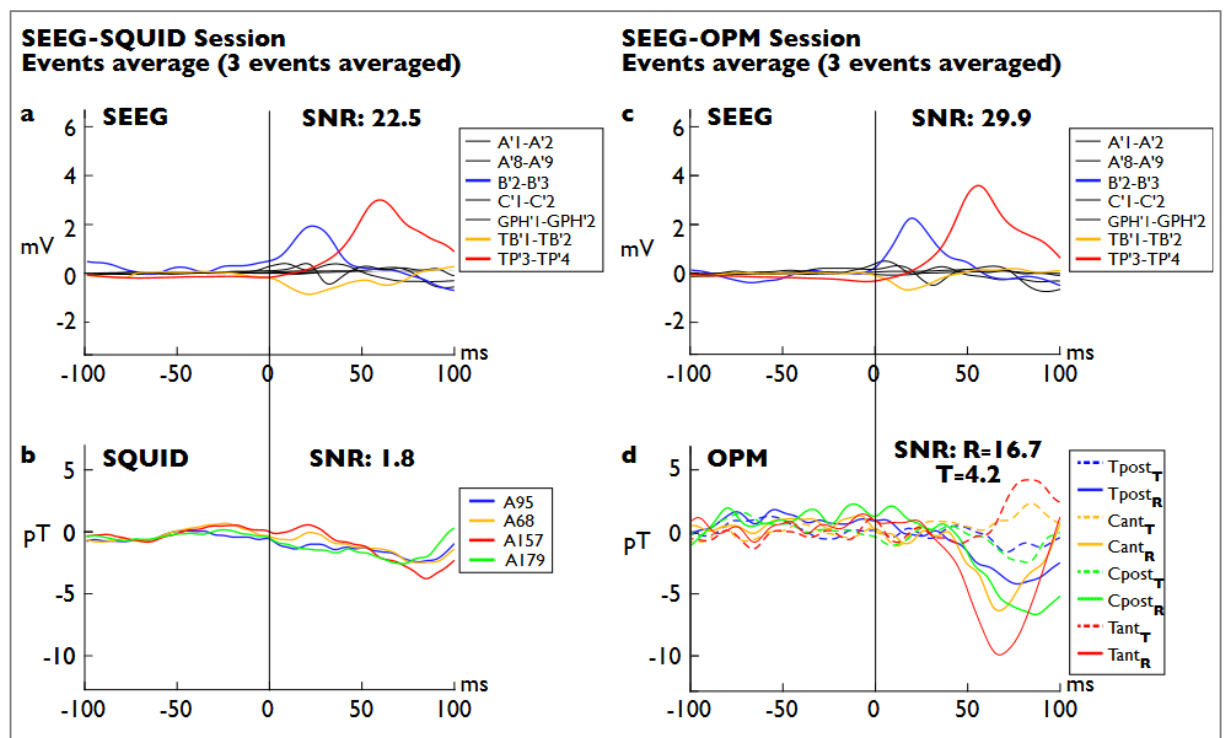
4

5 Fig. 3



1

2 Fig. 4



3